Typeset using LaTeX **two column** style in AASTeX62

Draft version February 18 2019

The Origin of Radio Emission from Radio-Quiet AGN

F. Panessa [1] R. D. Baldi [2 3] A. Laor [3] P. Padovani [4] E. Behar [3] and I. Mchardy[2]

[1] *INAF Istituto di Astro sica e Planetologia Spaziali, via Fosso del Cavaliere 100, I-00133 Roma, Italy*
[2] *School of Physics and Astronomy, University of Southampton, Southampton, SO17 1BJ, UK*
[3] *Physics Department, Technion, Haifa 32000, Israel*
[4] *European Southern Observatory, Karl-Schwarzschild-Str. 2, D-85748 Garching bei München, Germany*

ABSTRACT

The central nuclei of galaxies, where super-massive black holes (SMBHs) are thought to reside, can experience phases of activity when they become Active Galactic Nuclei (AGN). An AGN can eject winds, jets, and produce radiation across the entire electromagnetic spectrum. The fraction of the bolometric emission in the radio spans a factor of $\sim 10^5$ across the di erent AGN classes. The weakest radio sources, radio-quiet (RQ) AGN, are typically 1,000 times fainter than the radio-loud (RL) AGN, and represent the majority of the AGN population. In RL AGN, radio emission is essentially all produced by synchrotron emission from a relativistic jet. In contrast, in RQ AGN the absence of luminous jets allows us to probe radio emission from a wide range of possible mechanisms, from the host galaxy kpc scale down to the innermost region near the SMBHs: star formation, AGN driven wind, free-free emission from photo-ionized gas, low power jet, and the innermost accretion disc coronal activity. All these mechanisms can now be probed with unprecedented precision and spatial resolution, thanks to the current and forthcoming generation of highly sensitive radio arrays.

Keywords: Astronomy and astrophysics; astrophysical disks; astrophysical magnetic fields; time-domain astronomy; compact astrophysical objects

1. INTRODUCTION

The evolution of each massive galaxy in the Universe is strictly connected to the activity of the super-massive black hole (SMBH, 10^6 ^{1} $M_\odot$) located at its centre. The SMBH becomes active when surrounding material is captured by the BH gravitational potential well forming an accretion disc and occasionally ejecting plasma in the form of outflow and/or a collimated jet. In this phase, active nuclei emit light over the entire electromagnetic spectrum due to a large variety of physical mechanisms.

Only $\sim 10\%$ of Active Galactic Nuclei (AGN) possess the ability of launching powerful relativistic jets that shine in the radio band and emit synchrotron radiation (e.g., Begelman et al. 1984). These have been called Radio-Loud (RL) AGN, as the radio emission is typically 10^3 times brighter than that in Radio-Quiet (RQ) AGN[1]. However, a sharp separation between RL and RQ is hard to set, as AGN show a large variety of radio properties and morphologies, with sources exhibiting compact cores, jets, knots, and extended di use emission in a wide range of strengths and sizes ranging from sub-pc up to kpc and even Mpc scales. The radio emission from these components depends on frequency and on the AGN type.

Radio emission, especially at high frequencies, is highly penetrative (at variance with the optical and soft X-ray bands, which are heavily absorbed in at least half of the AGN) fostering an unbiased view of the AGN population. The radio power, morphology and spectral index provide an initial characterization of the emission, which largely depends on the spatial resolution of the used radio interferometer (arcseconds to milli-arcseconds, see Figure 1) and on the redshift of the source (local to high z). At low redshift, interferometric studies allow us to investigate the radio nuclear properties and to probe the plethora of physical mechanisms acting in RQ AGN, i.e., star formation (SF), accretion disc winds, coronal disc emission, low-power jets[2] or a combination of them (Fig. 2). Indeed, the relatively few

[1] The classical radio-optical radio-loudness parameter R is defined as f(4400 Å)/f(6 cm) (Kellermann et al. 1989), where RQ AGN have R $<$ 10. See also Terashima & Wilson (2003) for a radio–X-ray based definition R_X = L (6 cm)/L(2-10 keV).

[2] Here we use the 'jet' term to indicate an outflow that becomes collimated, whereas a 'wind' is an uncollimated outflow. Both transport outwards mass, energy and angular momentum.

available studies of RQ AGN at high and low resolution (e.g., Kellermann et al. 1989, 1994; Barvainis et al. 1996; Kukula et al. 1998; Ulvestad et al. 2005; Leipski et al. 2006; Padovani et al. 2011; Doi et al. 2011; Zakamska et al. 2016a,b; Hartley et al. 2019) have generally led to mixed results. This is not surprising, as all RQ AGN are powered by a SMBH and emit X-rays (from a corona), most are in star-forming hosts, and many display outflows.

In this review we discuss, using an observational approach, the physical mechanisms that in our opinion may significantly contribute to the radio emission in RQ AGN (Section 2), highlighting analogies and di erences between other radio-emitting astrophysical accreting systems (Section 3). In Section 4 we provide testable theoretical predictions to evaluate the dominant mechanism and in Section 5 we draw the required recipes for current and future radio facilities; we conclude with Section 6. We refer in general to RQ AGN with radio absolute weak powers and/or radio faint emission with respect to the emission at higher frequencies, including in this class RQ QSOs (RQQs), Seyfert galaxies and LINERs[3]. Our purpose in this review is to alert the general AGN community that the radio regime is becoming a powerful new tool for studies of a variety of physical mechanisms in RQ AGN, at unprecedented resolution.

2. PHYSICAL AND RADIATIVE MECHANISMS

Multiple physical radio-emitting processes are thought to be in act in the nuclear regions of RQ AGN (see Fig. 2 for a simple sketch). Below we discuss the observational evidence and interpretation related to each mechanism separately.

2.1. *Jets*

Ejected material from an accreting SMBH can take the form of highly collimated and powerful relativistic jets (Begelman et al. 1984), from pc to Mpc scales, emitting synchrotron emission and up-scattered photons via inverse Compton into X-rays and γ-rays. AGN jets display a broad variety of radio structures (for example FR I and FR II, Fanaro & Riley 1974), with a wide span of intrinsic powers.

Flat or slightly inverted radio spectra from very compact sources are generally associated with an optically thick launching region, such as a jet base (Blandford & Königl 1979; Reynolds 1982)[4], obtained from the overlap of magnetised self-absorbed synchrotron blobs or multiple components with an optically-thin low energy turnover (Falcke & Biermann 1995). The high-brightness temperature of radio cores is thought to be the result of non-thermal processes from relativistic electrons (Blundell & Beasley 1998). The size of the visible inner AGN jet cone scales proportionally with wavelength and is typically on the pc scale.

At low radio luminosities, follow-up radio surveys of optically selected nearby low luminosity AGN (LLAGN, with luminosities at 1.4 GHz below 10^{42} erg s ^{1}, including LINERS and low-luminosity Seyferts (Falcke et al. 2000; Ho & Ulvestad 2001; Nagar et al. 2002b; Nyland et al. 2016; Baldi et al. 2018; Chiaraluce et al. 2019) have yielded extremely high detection rates, with the radio emission having predominantly a flat spectrum, compact core morphology, occasionally accompanied by jet-like features on pc scales with intermediate resolution (1 0.1″ with VLA and eMERLIN). The radio emission on mas scales is often compact and most of the large scale radio emission is resolved out when imaged with the long-baselined arrays (Falcke et al. 2000; Nagar et al. 2001). In particular, Seyferts often display compact nuclear radio emission, occasionally similar to the jetted LINERs (see left panel of Fig 1) and more frequently similar to low-brightness di use lobed structures, indicative of sub-relativistic bulk speeds (e.g., Baum et al. 1993; Kukula et al. 1996; Gallimore et al. 2006; Kharb et al. 2014; Singh et al. 2015), as measured on pc scales in a few Seyferts (Roy et al. 2000; Middelberg et al. 2004). Long-baseline radio observations show that most Seyfert galaxies possess compact sub-pc scale nuclear emission with brightness temperature $>10^7$ K and occasionally misaligned pc-scale jets, possibly suggestive of jet precession (Middelberg et al. 2004; Giroletti & Panessa 2009; Panessa & Giroletti 2013; Kharb 2018).

Emission from RQ AGN has been sometimes explained with a scaled-down version of more powerful jets, where the di erence between RL and RQ could be due to a di erent efficiency in accelerating relativistic electrons on the sub-pc scale and in collimating the flow (Falcke & Biermann 1995). The jet properties likely evolve with the bolometric AGN luminosity. This results in a higher fraction of radio jets observed in local low-luminosity RQ AGN than in powerful quasars (Blundell & Rawlings 2001; Ho & Ulvestad 2001; Ulvestad & Ho 2001; Blundell 2003; Heywood et al. 2007; Baldi et al. 2018), although selection e ects may play a role. Radio

[3] In this work we do not enter into the details of the di erent RQ AGN classes but instead provide a broad view of radio emission in (mostly) local RQ AGN. For a recent and detailed discussion of AGN classification and an alternative naming of RL/RQ AGN as "jetted" and "non-jetted" AGN see Padovani et al. (2017) and Padovani (2016, 2017).

[4] Note that jet bases do not always have flat spectra, as in the case of some FR I sources (Laing & Bridle 2013).

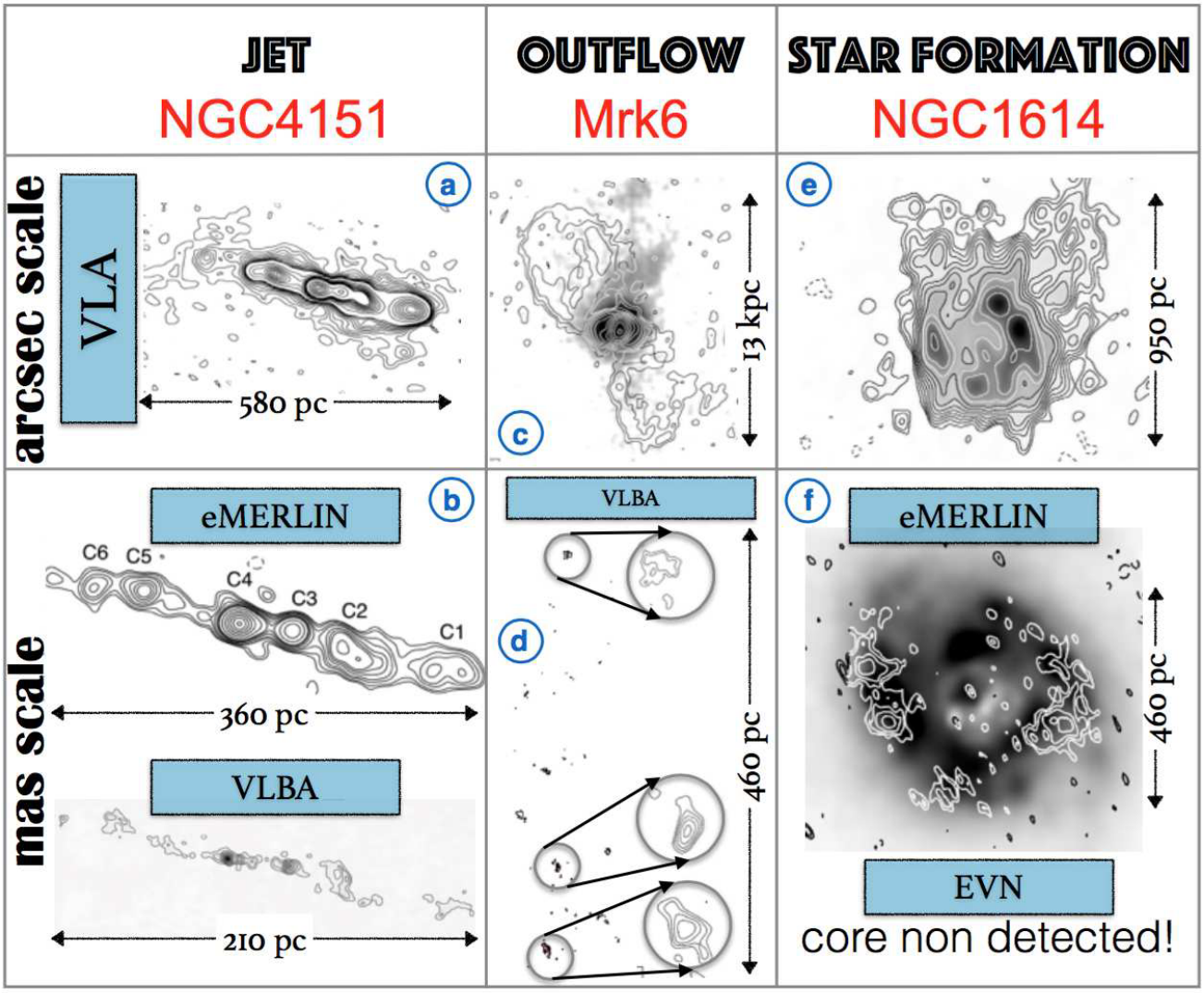

Figure 1 Prototype radio maps of RQ AGN with extended radio morphologies. Upper panel maps with arcsec resolution (from VLA) and lower panel maps with mas resolution: 8-GHz jetted structure of NGC 4151 (panel *a*, Pedlar et al. 1993), resolved in several components (panel *b*) with eMERLIN (Williams et al. 2017) and VLBA (Mundell et al. 2003) at 1.4 GHz; Mrk 6 at 1.5 GHz (panel *c*, Kharb et al. 2006) for an outflowing bubble-like structure resolved in smaller components with VLBA at 1.6 GHz (panel *d*, Kharb et al. 2014); NGC 1614 at 8.4 GHz (panel *e*, Olsson et al. 2010) from a star-forming di use structure, showing a clear ring with eMERLIN at 5 GHz (panel *f*, Olsson et al. 2010), no core detected with EVN at 5 GHz (Herrero-Illana et al. 2017).

structures of RQQ are found to be larger than those of Seyfert galaxies, but with similar morphologies (Leipski et al. 2006). Similarly, LINERs typically show core-brightened radio jets reminiscent of those observed in small FR Is (Capetti et al. 2017).

2.2. *AGN winds and thermal free free emission*

A rich and complex phenomenology of galactic winds located at di erent spatial scales has been revealed by multi-wavelength observations. Sub-relativistic (0.1 0.25 c) ultra-fast outflows (UFOs) in the vicinity of the BH (gravitational radius R_g scales) have been typically observed as Fe K-shell X-ray absorption-line features (Chartas et al. 2009; Tombesi et al. 2010; Pounds 2014; Nardini et al. 2015), as well as fast multiple components in soft X-ray grating spectra (Gupta et al. 2015; Longinotti et al. 2015). Lower velocities and temperatures from photo-ionised winds are detected in soft X-rays and UV spectra (Crenshaw et al. 1999; Laor & Brandt 2002). On kpc scales, broad and high velocity kinematic components are present in Seyferts and more luminous AGN as seen in [O III]λ5007 emission line profiles (Mullaney et al. 2013; Zakamska & Greene

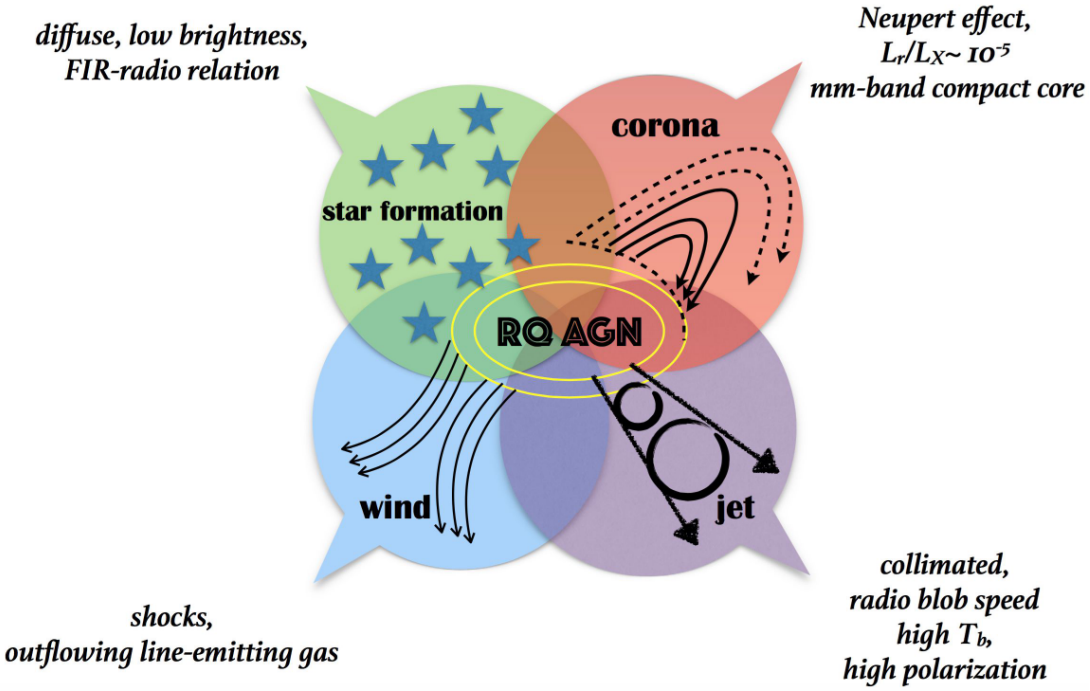

Figure 2 Sketch of the four main di erent physical mechanisms discussed in this work, to account for the origin of the radio emission in RQ AGN. For SF a di use low-surface brightness extended emission is expected, by tracing the host morphology, in significant excess with respect the FIR-radio correlation valid for quiescent star-forming galaxies (Sargent et al. 2010); the coronal emission would emerge from the optically-thin radio emission in case of a high radio frequency flat-spectrum unresolved core with a radio and X-ray luminosities consistent with the Guedel & Benz (1993) relation ($L_R/L_X \sim 10^{-5}$) and a specific dependence of the correlated radio–X-ray light curves, as predicted by the Neupert e ect (Neupert 1968); the measurements of the jet blob speeds, a high brightness temperature ($T_b > 10^8$ K) and high polarization are key parameters to identify a collimated jet emission; for a wind origin, shocks on the interstellar medium are expected to ionize the gas and emit blue-shifted X-ray, optical, and molecular lines, sign of the outflowing material.

2014) as well as in molecular outflows (Morganti et al. 2015), occasionally associated with di use radio emission (see middle panel of Fig 1). It has been suggested that compact radio emission plays an important role in disturbing the [O III] emitting gas in optically selected AGN (Capetti et al. 1999; Mullaney et al. 2013; Harrison et al. 2015). The correlation found in RQ AGN between radio emission and [O III] line velocity has been explained as the e ect of wind shocks (Fig. 3, Zakamska & Greene 2014), with an extension to the most luminous high-redshift quasars, as discussed by Hwang et al. (2018). Such shocks accelerate relativistic electrons producing synchrotron radio emission on scales > 100 pc, with powers at the level of those observed in RQ AGN, $\nu L \sim 10^{-5} L_{AGN}$ (Nims et al. 2015). In low-luminosity Seyferts, the base of the outflow is found to be coincident with the unresolved nucleus, pointing to the AGN as the predominant ionising source of the outflowing gas (Lena et al. 2015). Indeed, low-brightness temperature ($T < 10^5$ K) VLBI radio cores are consistent with an extended thermal origin from a small scale outflow (Christopoulou et al. 1997). In addition, the positional coincidence with low-luminosity water masers suggests that the radio continuum may arise from the inner regions of a molecular disc or from a nuclear wind (Gallimore et al. 2004; Hagiwara 2007).

Disc winds may also produce radio emission via bremsstrahlung free-free processes from an optically thin ionized plasma (Blundell & Kuncic 2007; Blustin & Fabian 2009; Steenbrugge et al. 2010). It has been shown that for a sample of quasars, free-free emission from a disc wind cannot mutually account for the observed radio and X-ray luminosities (Steenbrugge et al. 2011). However, simple emission measure estimates from the narrow line region gas indicate that the free-free emission of this gas may lead to detectable fluxes in the millimetre (mm) band (Baskin & Laor, in preparation).

Competing driving mechanisms have been proposed for AGN winds, such as starburst outflows (Heckman et al. 2015) and magnetic fields (Fukumura et al. 2010).

Supernovae, which are common in intense SF regions, can blow super-winds, which inflate radio bubbles. The energetic budget of these super-winds (Heckman et al. 2015) from high star formation rates (~30-50 $M_\odot$ yr $^{-1}$)

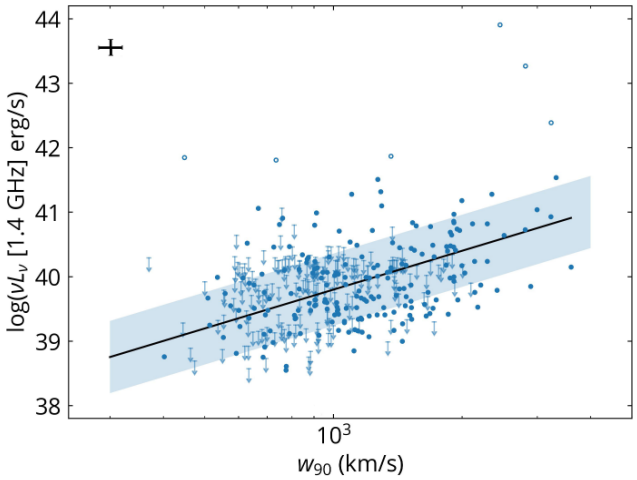

Figure 3 Radio luminosities at 1.4 GHz versus the velocity width containing 90 per cent of [O III] line for the low-redshift (z<0.8) type-2 quasars (Zakamska & Greene 2014), with radio luminosity upper limits from FIRST and NVSS surveys. The error bar at the top-left corner describes the typical uncertainties of the data. The black line is the quadratic fit on the low-z RQ sample and the shaded region represents the root-mean-square scatter. Figure adapted from Fig. 7 in Hwang et al. (2018) (courtesy of Nadia Zakamska).

appears to be able to account for the global properties of the ISM and the extended radio structures observed in several Seyferts and starburst galaxies (Veilleux et al. 1994; Genzel et al. 1995; Maiolino et al. 1998; Kharb et al. 2006).

Magneto-hydrodynamic (MHD) accretion-disc winds have been proposed to explain the wide variety of X-ray winds (Fukumura et al. 2014). Interestingly, UFOs have been observed both in RQ and RL AGN (e.g., Tombesi et al. 2011; Longinotti et al. 2015), suggesting that jets and winds may co-exist (Giroletti et al. 2017), contrary to BH X-ray Binaries (XRBs), where the presence of an accretion disc wind is observed only during the softer X-ray states (see Section 3) and could be responsible for the quenching of the radio jet (Ponti et al. 2012, see also NS binaries Díaz Trigo & Boirin 2016). On the theoretical side, MHD models predict the possible co-existence of jets and winds, suggesting that an axial collimated jet of low matter density and an extended disk wind maybe both part of the same outflow (e.g., Ferreira et al. 2010). The former is likely connected to the BH, while the latter arises from the inner regions of the accretion flow (Tchekhovskoy et al. 2011).

2.3. *Accretion Disc Coronae*

The presence of a hot $T \sim 10^9$ K corona in the vicinity of BH accretion discs has been suggested as early as fifty years ago to explain the non-thermal (Comptonised) X-ray spectrum, first for stellar BHs (Shapiro et al. 1976) and later for AGN (Haardt & Maraschi 1991). Compared to other potential radio sources in the AGN and host galaxy, the coronal component comes from the smallest region around the BH, i.e., 10–10,000 R_g (about a milli-pc for a BH of 10^8 $M_\odot$). Consequently, it is largely unresolved by contemporary instruments, and its size needs to be assessed from models or variability, as discussed below.

A first hint that radio emission from RQ AGN is related to the central nuclear source comes from the correlation of the radio luminosity L_R and the X-ray luminosity L_X (Brinkmann et al. 2000; Salvato et al. 2004; Wang et al. 2006; Panessa et al. 2007; Panessa & Giroletti 2013; Panessa et al. 2015). The strongest evidence comes from the Palomar-Green (PG) quasar sample ($z < 0.5$, Boroson & Green 1992), where it was found (Laor & Behar 2008) that L_R at 5 GHz and L_X (0.2 – 20 keV) are not only correlated over a large range of AGN luminosity, but follow the well established relation for coronally active cool stars of $L_R/L_X \sim 10^{-5}$ (Guedel & Benz 1993). The origin of this relation is not well understood from first principles in stars either, but it may suggest a coronal, magnetic origin for the radio emission in RQ AGN from magnetic reconnection phenomena.

The size in pc, $R_{\rm pc}$, of a self-absorbed synchrotron source, assuming a circular optically thick spot on the sky, decreases with frequency according to the equation derived from Laor & Behar (2008) (eq. 19 therein):

$$R_{\rm pc} \simeq 0.54 L_{39}^{1/2} \nu_{\rm GHz}^{7/4} B^{1/4} \qquad (1)$$

Hence, the 5 GHz emission likely comes from the broad line region scale, of about $10^4 R_g$. Observing the radio corona at scales comparable to those of the X-ray source ($\sim 10\ R_g$) requires observing at much higher frequencies (Behar et al. 2015) in the mm band at 100 – 300 GHz. At higher frequencies, cold dust emission from the host dominates. At 100 GHz (3 mm), flux densities have been measured for a few dozen local AGNs (Behar et al. 2015, 2018), and found to exceed the interpolation of the low-frequency steep slope power-law. Source sizes were estimated from Eq. (1) to be of less than a light day, and between 10 and 1000 Rg, which is comparable to the variability size of the X-ray source. Detections of mm excess in Seyfert galaxies confirm the interpretation of a compact, optically thick core that is superimposed on the steep power law of more extended structures that dominate at lower frequencies (Inoue & Doi 2014; Doi & Inoue 2016; Inoue & Doi 2018). Recently, Inoue & Doi

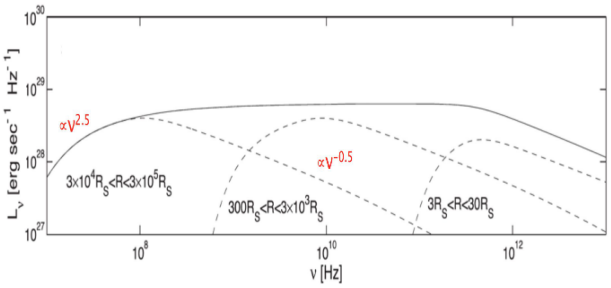

Figure 4 The spectrum of a distribution of power-law electrons in a spherical corona. The solid line represents the overall emission, and the dashed lines the contributions of the di erent spherical components at di erent gravitational radii. The specific intensity increases with the frequency as $\propto$ $^{2.5}$ in the optically thick regime at low frequency and decrease as $\propto$ $^{.5}$ in the optically thin regime at high frequency. Figure adapted from Fig. 4 of Raginski & Laor (2016).

(2018) reported the detection of coronal synchrotron radio emission from two nearby Seyfert galaxies associated with a magnetic field of ~ 10 Gauss on scales of $\sim 40\ R_g$ from the central BHs. Theoretical computations (Raginski & Laor 2016) explored this conjecture quantitatively showing that an X-ray corona can produce a flat synchrotron radio spectrum up to a break at 300 GHz or higher (Fig. 4).

The smoking gun of the coronal origin of the radio emission in RQ AGN would be the detection of the radio and X-ray variability correlation observed in stellar coronae, the so-called Neupert e ect (Neupert 1968; Güdel et al. 2002) in which the radio flare precedes the X-ray one, and over the duration of the flare the time derivative of the X-ray light curve varies in a fashion similar to the radio light curve $L_R \propto dL_X/dt$. This is interpreted as a result of energetic electrons that emit synchrotron radio ($\propto L_R$) depositing their heat in the corona that subsequently shines out the *total* energy in X-rays, thus $L_X \propto \int L_R dt$, and hence the observed correlation.

Flares and dips in the hard (jetted) state of X-ray binaries have shown a related e ect of $L_{opt} \sim -dL_X/dt$, where L_{opt} is the optical luminosity coming from synchrotron emission (Malzac et al. 2003), but where the minus sign makes it di erent from the Neupert e ect. Indeed, Malzac et al. (2004) interpret the e ect in terms of a jet-disc coupling and a common energy source for the synchrotron jet (optical emission) and the Comptonizing electrons (X-rays), so that one is enhanced at the expense of the other and vice versa. The analogy to AGNs is unclear yet intriguing, and should be studied further as more multi-wavelength observations of RQ AGN become available (see Section 3).

2.4. *Star formation*

SF is the process by which dense regions within molecular clouds in the ISM collapse and form stars. SF activity produce thermal and non-thermal radio emission thanks to the presence of strong magnetic fields and hot plasma from supernova remnants and cosmic rays. Star-forming regions are typically host-like extended, di use, clumpy and with low surface brightness (see a clear example in the right panel of Fig. 1 and others in Orienti et al. 2015). The SF phase, in particular, is characterised by steep GHz spectra ($_r \approx 0.7$) dominated by synchrotron emission at low frequencies with a flat free-free component, which becomes predominant at ν 30 GHz (Condon 1992).

Far-Infrared (FIR) emission, indicator of dust and cold gas, an ideal cradle for new generations of young stellar populations, has been found to correlate with radio emission for Seyferts and relatively low-redshift RQQ, which follow the so-called FIR – radio correlation typical of star-forming galaxies (SFGs) (Sopp & Alexander 1991; Sargent et al. 2010), which is understood to be driven by recent SF. In addition, the FIR flux density in Seyfert galaxies correlates better with the low-resolution kpc-scale radio flux density rather than with the high-resolution pc-scale emission (Thean et al. 2001), which points to an SF origin for the former at the galaxy scale. All of the above fits with the fact that low-luminosity RQ AGN are usually hosted in late-type galaxies, which are commonly star-forming.

The situation at higher powers (and redshifts), however, is not so clear-cut, as discussed by Padovani (2016). On the one hand, it appears that the main contribution to radio emission in sub-mJy RQ AGN selected at 1.4 GHz at $z \sim 1.5$ comes from SF activity in the host rather than from the AGN (e.g., Bonzini et al. 2015; Padovani 2016; Delvecchio et al. 2017; Gürkan et al. 2018). This scenario is based on the fact that the SF rate derived from the FIR luminosity as traced by *Herschel* agrees extremely well with that estimated from the radio power under the assumption that the latter is due to SF (Bonzini et al. 2015, see Fig. 5). This is further supported by: i) the fact that Extended *Chandra Deep Field*-South (E-CDFS) RQ AGN occupy the same locus as SFGs also in the SF rate (SFR) – stellar mass plane (Fig. 5 of Bonzini et al. 2015); ii) the similar radio luminosity evolution of E-CDFS RQ AGN and SFGs (Padovani 2016); iii) the L_R/L_X ratios of E-CDFS RQ AGN, which show higher values than those expected for coronal emission (Sect. 2.3) and synchrotron emission from AGN outflows (Nims et al. 2015, and Sect. 2.2), but smaller than the corresponding ratios for relativistic jets. Moreover, the radio sizes of radio-selected AGN

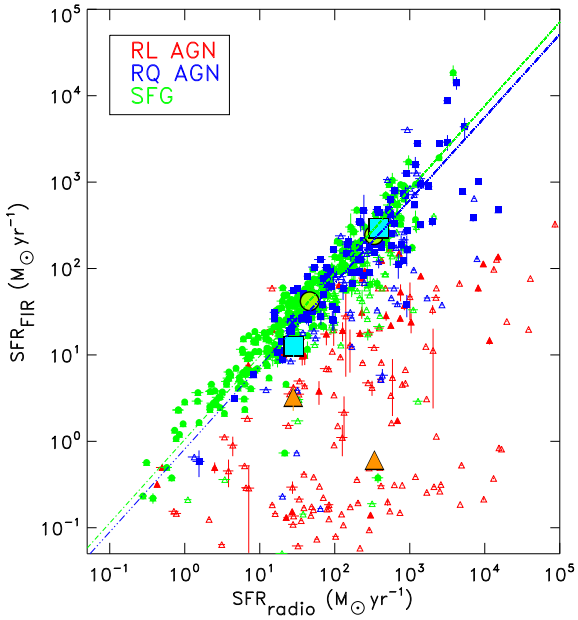

Figure 5 SF rate derived from the FIR luminosity versus the SF rate from $P_{1.4\mathrm{GHz}}$ for the E-CDFS sample. SFGs are plotted as green circles, RQ AGN as blue squares, and RL AGN as red triangles. Full symbols represent sources detected in at least one Photoconductor Array Camera and Spectrometer (PACS) filter, while sources shown as empty symbols are *erschel* non-detections, for which $\mathrm{SFR_{FIR}}$ is less robust. Large symbols with lighter colours are the results of a stacking analysis. The two lines are the best fits for the SFGs and RQ AGN with PACS detection. Error bars denote the uncertainties on the derived SF rates. Figure reproduced from Bonzini et al. (2015), Fig. 3, with permission.

with $\mathrm{SFR_{radio}} \approx \mathrm{SFR_{optical\ FIR}}$ are typically a factor of 2 larger than those for which $\mathrm{SFR_{radio}}$ exceeds by more than 3σ $\mathrm{SFR_{optical\ FIR}}$ (Bondi et al. 2018). This is fully consistent with SF-related radio emission in the former sources. A core, possibly BH-related component, however, can also be present in radio-selected RQ AGN, which clearly show extended SF in other bands (see also Sect. 2.1 for local sources). Some sub-mJy RQ AGN, in fact, show evidence for relatively strong compact radio cores (e.g., Chi et al. 2013; Maini et al. 2016; Herrera Ruiz et al. 2016), which suggests that the AGN component might be at the same level as, or even stronger than, the SF one. In addition, SFGs can hide LLAGN at their centre able to launch pc-scale radio structures (Baldi et al. 2018). At higher resolutions, one needs to keep in mind, though, that VLBI detections are still biased towards AGN-dominated sources, resulting in an incomplete view of the SF at the nuclear scale.

On the other hand, di erent results can be obtained for RQ AGN samples selected in other bands (see also Sect. 2.3 for the PG sample). Zakamska et al. (2016a) have come to the conclusion that radio emission in their sample (optically selected, $S_{1.4\mathrm{GHz}} > 1$ mJy, $z < 0.8$, and $L_{\mathrm{bol}} > 10^{45}$ erg s ^{1}) is dominated by quasar activity, not by the host galaxy (see also White et al. 2017). However, Kellermann et al. (2016), by studying $0.2 < z < 0.3$ optically selected quasars at 6 GHz, agree with the results obtained from the E-CDFS sample. One might think that power might play a role, since E-CDFS RQ AGN have relatively low luminosities ($\langle L_{\mathrm{x}} \rangle \sim 10^{43}$ erg s ^{1} i.e., $L_{\mathrm{bol}} \approx 3 \times 10^{44}$ erg s ^{1}; see also Rosario et al. 2013, who find similar results to Bonzini et al. 2015). Other complicating issues might include di erent definitions of RQ/RL AGN, and the radio frequency at which the studies are made[5].

3. COMPARISON WITH OTHER ACCRETING SOURCES

A possible pathway towards the understanding of the mechanisms producing radio emission in RQ AGN is through the comparison with other accreting sources, from Young Stellar Objects (YSOs), to XRBs (either BHs or neutron stars) and active SMBHs. These various accreting sources display substantial di erences, e.g., in the central mass, outflow velocities, disc temperatures, energy output and magnetic fields. However, a number of common features and parameters (e.g., disc morphology, degree of collimation, ejection velocity and direction) has led to the suggestion that they may all share similar physics in the phenomenon of accretion and ejection (Price et al. 2003).

From XRBs we have learnt that jets and outflows are intermittent in their nature, likely following accretion state changes (Fender et al. 2004; Ponti et al. 2012). Di erent attempts have been made to unify XRBs with AGN (Falcke et al. 2004; Körding et al. 2006). More specifically, XRBs in their low-accretion rate hard state, can launch jets (with moderately relativistic speeds), similar to AGN. In this state, the observed relationship between their X-ray and radio luminosities (Corbel et al. 2003; Fender et al. 2004) provide evidence for a physical connection between the inflow and the collimated outflow. Conversely, in the higher accretion rate 'soft state' no evident radio activity has yet been found despite very deep searches (Russell et al. 2011). Strong radio flares are often detected through the transition

[5] At low frequencies the steep synchrotron SF-related emission dominates, while at higher frequencies a flat component from a radio core or a corona should be relevant (Sects. 2.1 and 2.3; but note that the Zakamska et al. 2016a results were obtained at 1.4 GHz, as the E-CDFS ones; and, moreover, as discussed above, at high frequencies a flat component is expected also from SF).

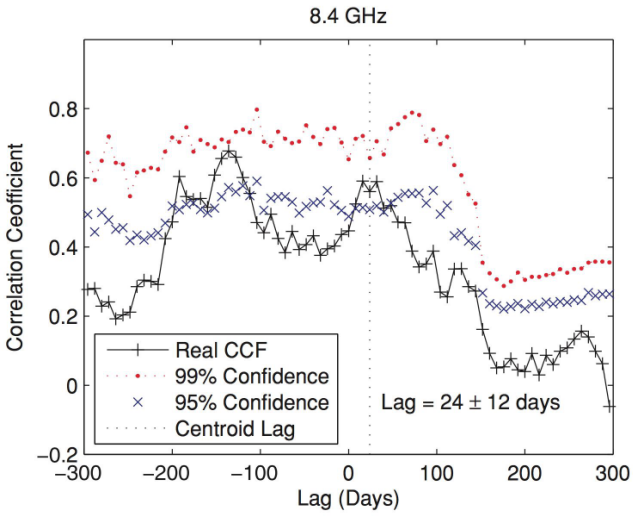

Figure 6 Discrete cross-correlation function plot showing time-lag against the correlation coefficient for X-ray to radio (8.4 GHz lagging X-ray) (black crosses) for NGC 7213. A time lag of 24 12 d is found to maximise the cross-correlation function. The 99 and 95 per cent local significance confidence levels are plotted (reproduced Fig. 2 from Bell et al. 2011).

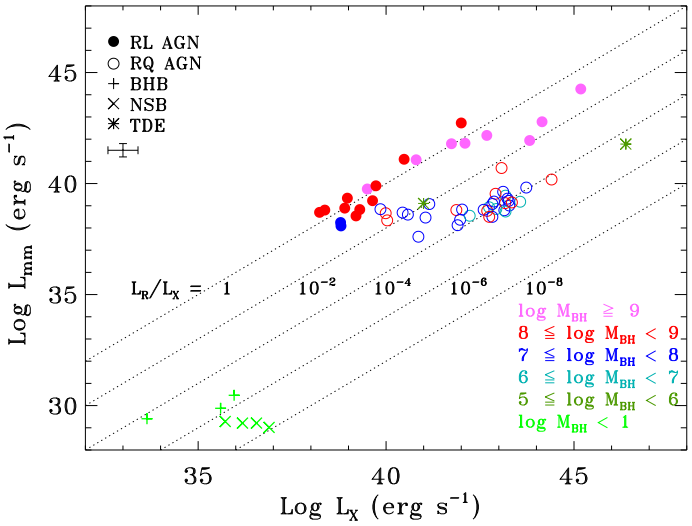

Figure 7 X-ray luminosity (2-10 keV, erg s^{-1}) versus mm-band luminosity (90-100 GHz, erg s^{-1}) for RL AGN (Hardcastle & Looney 2008; Cotton et al. 2009; Doi et al. 2011), RQ AGN (Doi et al. 2011; Behar et al. 2015, 2018), XRBs (BH and neutron star binaries, Fender et al. 2000; Berger et al. 2012; Yuan et al. 2016; Díaz Trigo et al. 2017, 2018; Tetarenko et al. 2018a,b) and TDEs (IGR J12580+0134 and SWIFT J1644+5734). We colour the symbols based on the BH masses ($M_\odot$) derived from stellar velocity dispersions. For AGN the observations in the two bands are not simultaneous, while for the other classes of sources, which are known to be transients, the data are taken on the same day or a few days apart. Precisely, we include XRBs (V404 Cyg, Cyg X-1, Aql X-1, 4U 1820-30, and MAXI J1820+070) in hard states and transitioning to soft states. The dashed lines correspond to L_{mm}/L_X of 1, 10^{-2}, 10^{-4}, 10^{-6}, and 10^{-8}. In the upper-left corner, the plot legend includes the typical error bar associated with the data-points. Figure updated and adapted from Fig. 3 of Behar et al. (2015).

between the two states at high accretion rates, in some cases resolved into discrete symmetric blobs of material. A complex radio X-ray relationship can be observed during these transitions, involving an X-ray dip preceding a radio flare (Belloni et al. 1997; Mirabel et al. 1998), similarly to what is seen in the radio galaxy 3C 120 (Marscher et al. 2002; Chatterjee et al. 2009).

RQ AGN have shown cm/mm-band variability on day-month-year timescales (e.g., Wrobel 2000; Barvainis et al. 2005; Chatterjee et al. 2009; Mundell et al. 2009; Baldi et al. 2015), which, at face value, appears to be similar to the behaviour of binaries in their hard states. Nevertheless, simultaneous radio/X-ray monitorings are rare and have so far yielded only weak or no correlations, with ambiguous results (see Figure 6, Bell et al. 2011; King et al. 2011, 2013; Jones et al. 2011, 2017).

In the light of a possible unification of radio AGN with low/hard state XRBs, relevant models relating jet radio luminosity to the BH mass and accretion rate were proposed (Marko et al. 2001; Yuan et al. 2002; Heinz & Sunyaev 2003) to account for the accretion-ejection phenomenon in compact objects. Further observational support for such models is the so-called 'fundamental plane' (FP) of BH activity, relating mass, radio luminosity (at 5 GHz, 6 cm) and X-ray luminosity (e.g., Merloni et al. 2003; Falcke et al. 2004) which unifies XRBs, RL and RQ AGN. The scatter around the plane is substantial but is reduced if only low accretion rate BHs are considered (e.g., Körding et al. 2006; Falcke et al. 2004; Plotkin et al. 2012).

The wealth of incredible details known on jets and outflows structures and chemistry in YSOs could ease our comprehension of such phenomena in all accreting systems. Indeed, most jet parameters are derived from imaging and spectroscopy (e.g., velocity, mass loss rate, composition) and information on strength and direction of the magnetic fields would provide an almost complete characterization of outflows in YSOs. However, the radio emission observed is mainly non-thermal (Tobin et al. 2015). In this respect, YSOs and AGN complementary studies are of high value, as magnetic fields in AGN can be tested via polarisation. Similarities can be drawn between YSOs and both AGN and XRBs, such as the detection of proper motions or the birth of new radio knots ejected in this case by the star (e.g., Osorio et al. 2017). In addition, in YSOs the accretion is episodic

with periods of quiescence as suggested by the outflow structures (Bally 2016) and strictly connected to the ejection flow.

Hints of disc/jet coupling are found also in weakly accreting sources such as cataclysmic variables (Körding et al. 2008), as well as in highly accreting systems such as Ultra Luminous X-ray sources (Roberts 2007; Cseh et al. 2015; van den Eijnden et al. 2018) and Tidal Disruption Events (TDEs, Dai et al. 2018). In particular, TDEs o er the opportunity to observe in real time the on-set of jet activity at high (Bloom et al. 2011) and low power (Pasham & van Velzen 2018; van Velzen et al. 2016; Alexander et al. 2016, 2017; Mattila et al. 2018). The detection of a cross-correlation between the X-ray and radio light curves in the case of the TDE ASASSN-14li suggests that the soft X-ray emitting disc regulates the radio emission, providing evidence for disc-jet coupling also in recently formed jets (Pasham & van Velzen 2018).

As an attempt to unify the di erent accreting classes, in Figure 7 we plot the mm-band luminosity (∼3 mm) versus the X-ray luminosity (2–10 keV) for RQ and RL AGN, XRBs (BHs and neutron stars), and TDEs, coloured in bins of BH masses. Since the mm-band emission is expected to come from inner regions with respect to its cm-band counterpart (by a factor ∼200, see Eq. 1), the mm/X-ray luminosity ratio should be more representative of the properties of accretion and ejection in compact objects. This plot is only exploratory as mm-band observations are available only for a few sources so far and objects in di erent accretion states are considered. However, there is a clear displacement between RL and RQ AGN by 3-4 orders of magnitude at a given L_X. Furthermore, a dependence of the mm/X-ray ratio on BH mass is also evident, with the small BH masses showing lower ratios, as also found in the FP (Merloni et al. 2003). While TDEs shows mm/X-ray ratios similar to AGN, XRBs have even lower ratios, probably due to their smaller masses (note that several uncertainties are associated with the extremely object-dependent behaviour of XRBs).

4. TESTABLE THEORETICAL PREDICTIONS

In Figure 8, we present a scheme that could serve as a guide to evaluate which is the dominant physical mechanism in a RQ AGN radio map, by means of its morphology and spectral slope. Testable predictions can be drawn from simple arguments linked to the examined physical processes in this work and based on their main characteristics (see Figure 2).

In case of a jet origin, the physical mechanism may be similar to that of a RL jet ejection process, but scaled-down in luminosity by a factor of $\sim 10^3$. High resolution (i.e. with VLBI) observations may resolve the mas-scale jet structure and measure high-brightness knots motions for a larger number of sources viewed face-on, while for those viewed pole on, the emission may remain unresolved also on mas scale. Fundamental properties of the non-thermal emission component can be derived via radio observations, such as an estimate of the magnetic field (e.g., from frequency break in the spectra such as in Bontempi et al. 2012 or spectral energy distribution fitting as in Inoue & Doi 2018) and the degree of polarisation (Giroletti et al. 2005).

Extended di use radio emission may also be due to a wind-induced shock. Since AGN emission is non-isotropic, the wind is also expected to show some conical or double-lobed structure, in contrast with the host SF. Such a wind will inevitably manifest itself through the kinematics of spatially extended line emission (Veilleux et al. 2005) with a potentially strong impact on the galaxy (Harrison et al. 2018). The advantage of the radio band is that it allows us to probe the wind well down to sub-arcsec scale, otherwise accessible only with optical-IR space telescopes and interferometers or integral-field spectrographs.

Thermal free-free emission is simple to identify through its flat spectral slope of $L \propto \nu^{\cdot 1}$, with a typical brightness temperature of 10^4 10^5 K. Its luminosity could be calculated accurately based on the observed emission line luminosities. The free-free emission may be best probed at 100 200 GHz, before the thermal tail of the dust emission starts to dominate.

If the radio is produced in magnetised plasma in the accretion disc corona, as suggested by the observed $L_R/L_X \simeq 10^{\ 5}$ relation, then a robust prediction is that a compact sub pc, optically thick, flat spectrum source should emerge at high radio frequencies. The mm emission is expected to originate from a few R_g, and thus overlap the X-ray emitting region. The emission in the two bands is expected to correlate perhaps according to the Neupert e ect, where $L_R = dL_x/dt$, as detected in stellar coronae (see Sec. 2.3).

In analogy with coronally active stars, Coronal Mass Ejections (CMEs) may occur in the AGN coronae, which would also emit extended optically-thin radio emission in a form of outflowing blobs of highly magnetised plasma. This phenomenon would be more intense in very active coronae, which are expected to be in high-Eddington accretion discs (see Laor et al. 2019). If the CME speeds are highly subluminal, the jet model would coincide with the CME phenomenon and the jet base would physically coincide with the corona (see also Merloni & Fabian 2002; Liu et al. 2014; King et al. 2017).

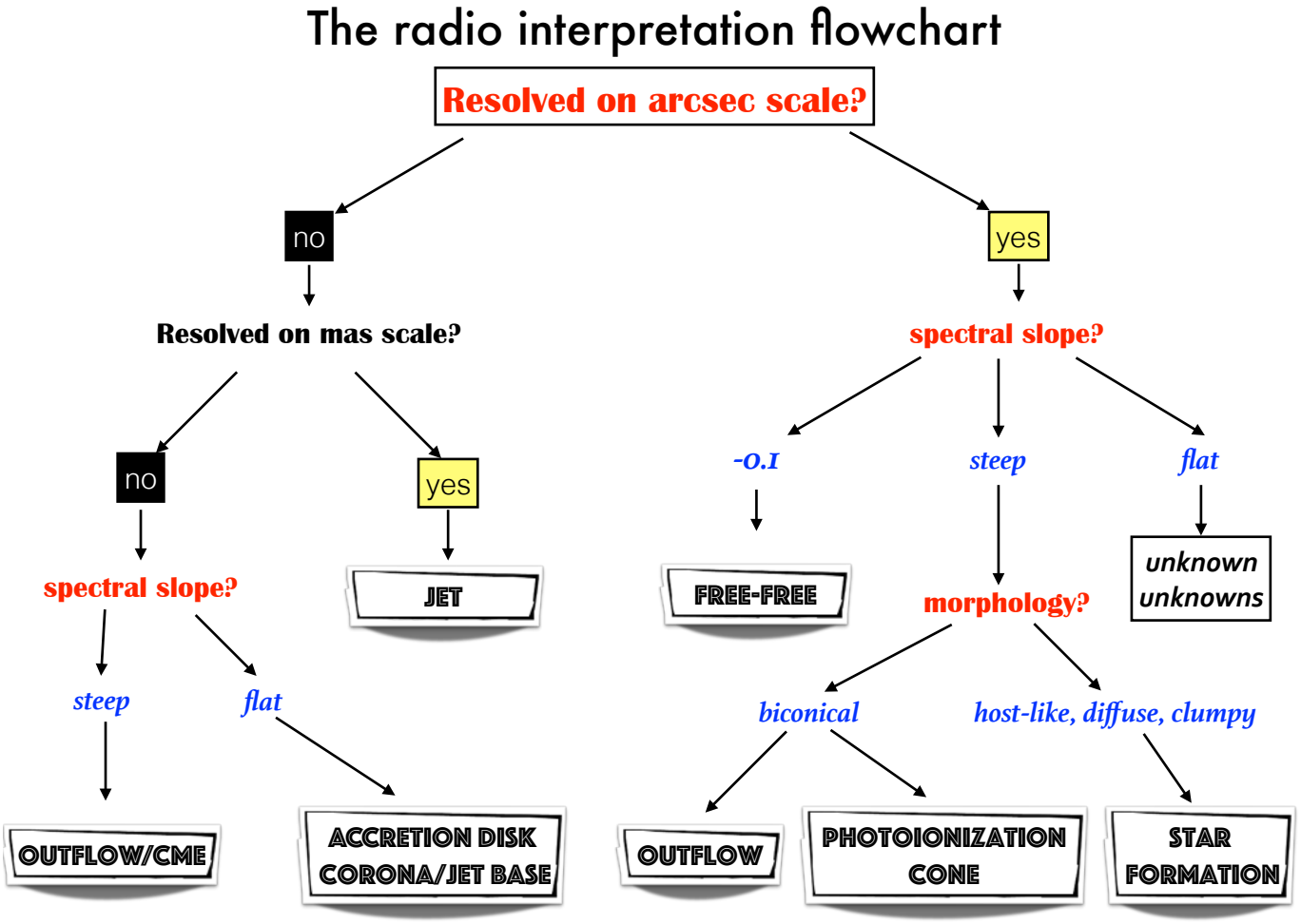

Figure 8 Flow chart to guide the interpretation of the radio emission in local RQ AGN. The size of the resolved radio emission at di erent resolution (arcsec and mas scales corresponds to kpc and pc scales, respectively for local galaxies), the surface brightness of the emission and the typical spectral slope derived between 1.4 and 8.5 GHz can be used as key parameters to approximately identify the di erent physical process involved in the radio band.

Radio emission produced by the SF will inevitably form a smoothly distributed host-like extended emission, which is obviously non-variable, and characterised by a steep spectral slope. The SFR in AGN host galaxies in the local Universe may reach $\sim 300 M_{\odot}$ yr ^{1}. At such a high SFR the Supernovae rate reaches a few per year. This raises the exciting possibility of follow-up deep VLBI observations of nearby AGN ($z < 0.1$), which show di use radio emission consistent with SF, and try to detect compact sources on the pc scale. It may be possible to detect individual SNe and SN remnants, as impressively done for the nearby ULIRGs M 82, Arp 220 and Arp 299-A (Muxlow et al. 1994; Batejat et al. 2011; Pérez-Torres et al. 2009). If doable, it will allow us to measure directly the SFR rate of massive stars very close to the centre.

The cleanest diagnostic of the various possible emission processes is the comparison of X-ray and radio flux variations. Correlated and lagged variability will provide strong support for the radio and X-ray sources being physically related and specific radio/X-ray time lags might point to a common origin. If radio emission comes from a synchrotron jet, we expect an X-ray/radio correlation, such as that seen in XRBs (e.g. Corbel et al. 2013). Assuming a scaling with BH mass, a jet origin would predict the low frequency radio to lag behind the X-ray photons in RQ AGN by tens of days as found in the RQ NGC 7213 (24 days radio lag, Fig 6, Bell et al. 2011). In contrast in the mm range, where the innermost disc becomes optically thin, one may observe the variability pattern seen in the solar corona, where magnetic field reconnection events lead to rapid particle acceleration and the production of radio emission,

causing X-ray emission (cooling) related to the integral of the radio emission (heating) and to lag behind the radio. Conversely, in the case of SF, radio and X-ray emission will not vary on years time-scales. Winds occur at di erent spatial scales and on di erent physical conditions, detailed modeling for the expected radio/X-ray correlated variability is still at its dawn.

5. NEAR-FUTURE DESIRED OBSERVATIONS

Significant improvement in this field could already be achieved with the current radio telescopes in a short-term future, ideally requiring: i) a complete and statistically meaningful sample of RQ AGN which covers a large range of radio luminosities and accretion rates, achievable by reaching μJy flux-density levels with short exposure times (i.e., $\sim$ 30 min of total time with array-A VLA to reach a sensitivity of 10μJy beam ^{1} and 0.4$''$ resolution at 5 GHz; $\sim$ 1 hour for eMERLIN at 5 GHz for a sensitivity of 25μJy beam ^{1} and 0.04$''$ resolution); ii) a full spectral coverage from cm band to FIR to discriminate between the di erent emission mechanisms (i.e., combining cm-band VLA and mm-band ALMA data, see Doi et al. 2011, 2013; Inoue & Doi 2018); iii) multi-scale (arcsec to mas-resolution) imaging to map and resolve the di erent emission structures from the galaxy to the innermost regions and trace their connection. In this respect, very-long baseline radio arrays have been implemented in the recent years with the possibility to combine them together in the Global VLBI network[6], allowing us to reach unprecedented angular resolution (up to 45 μarcsec) and *uv* coverage. An optimal technique, though not much exploited, is the combination of visibilities from short and long baselines obtained for example with VLA and eMERLIN. This procedure could probe intermediate scales in the *uv* plane, ideal for studying pc-scale extended radio emission in RQ AGN, which would be resolved out at long baselines and unresolved at short baselines.

The advent of the new radio facilities with unprecedented large collecting area, radio frequency coverage and angular resolution (i.e. LOFAR, SKA, ngVLA, EHT, ALMA, space VLBI; van Haarlem et al. 2013; Carilli 2015; Murphy et al. 2017; Gurvits 2018), which will be $\sim$50 times more sensitive and 10^4 times faster in the case of the SKA (sensitivity of 0.4 mJy beam ^{1} in one minute between 70 and 300 MHz), will represent the springboard to a new era of radio science. At μJy-level flux densities, the fraction of RQ AGN significantly increases implying that large numbers of these sources will be detected (a survey reaching $\sim$ 1 μJy at $\sim$ 1 GHz over 30 deg^2 will detect $\approx$ 200,000 RQ AGN: Padovani 2016). SKA1 will be able to map the sky and reach a brightness temperature of 0.2 K at 10 GHz with sensitivity of 15 μJy arcsec ^{2} for 1000 hr observations with a 0.1$''$ synthesised beam (Dewdney et al. 2013). These values correspond to detecting galaxies forming stars at $\sim$100 and 10 M$_\odot$ yr ^{1} at all redshifts and a radio luminosity of $\sim 10^{33}$ erg s ^{1} at z=0.3 (1.6 Gpc; Murphy et al. 2015). Future facilities will enable polarization studies of faint sources, that can reveal the geometry of the compact radio emission and favour or disfavour magnetically-driven mechanism. Long-baseline high sensitivity facilities will allow high positional accuracy measurements in order to detect the motions of sub-relativistic radio blobs (minimum detectable size corresponds to a length of $\sim$1.6 light-years at z = 0.15 with a resolution of 1 mas, Paragi et al. 2015)

Short time investment on the new radio facilities at high radio frequencies could resolve mas-scale μJy-level radio components in galactic and extra-galactic sources. This will open up an uncharted radio sky, ready to be followed up by other new international facilities at shorter wavelengths (i.e., LSST, Euclid, WFIRST, ELTs, JWST, SPICA, eROSITA, Athena), providing multi-frequency monitoring campaigns with short and long visit cadences.

6. SUMMARY AND OUTLOOK

Radio astronomy is witnessing a golden age thanks to the large number of already available interferometers and to the high throughput of upcoming new facilities. RQ AGN become the dominant AGN radio population at flux densities below $\approx$ 0.1 mJy at 1.4 GHz (e.g., Padovani 2016). However, it is not only about quantity, but also about quality: nuclei can be investigated in their exciting variety of physical mechanisms in act. Accretion of material and consequent ejection of plasma, coronal activity, interaction with the surrounding medium and star-formation are the major sources of radio emission in this class of objects. Disentangling the above physical processes (or discovering new ones!) is difficult. Characteristic observational signatures can be identified for each process (although degeneracies are common) and testable predictions are within the reach of the current and future radio (including mm band) interferometers. The e ort that the di erent observational communities should undertake is to boost the multi-frequency approach, by simplifying the access to the time domain astronomy and to intensify the global observatory network to finally enable simultane-

[6] The combination of the European VLBI (EVN) and VLBA is known as Global VLBI (https://www3.mpifr-bonn.mpg.de/div/vlbi/globalmm/).

ous multi-band campaigns. Furthermore, there is urgent need to bridge the di erent astrophysical communities perspectives, from stars to SMBHs: accretion, ejection, coronae, winds and star formation are basic ingredients in most accreting systems, as well as in the accretion history of the Universe.

This review is the result of several fruitful discussions raised during the meeting 'The radio–X-ray connection in accreting objects' (21-25 May 2018, Tenuta Monacelle, Monopoli, Italy). The authors wish to thank all the participants to the meeting: John Bally, Niel Brandt, Gianfranco Brunetti, Alessandro Capetti, Stephane Corbel, Lixin Dai, Jordy Davelaar, Barbara De Marco, Jonathan Ferreira, Jose Gomez, Martin Hardcastle, Yoshiyoki Inuoe, Miranda Jarvis, Preeti Kharb, Amy Kimball (in particular for her original idea that inspired Figure 2), Mike Koss, Carol Mundell, Dheeraj Pasham, Uria Peretz, Manel Perucho, Richard Plotkin, Isabella Prandoni, Juri Poutanen, Tim Roberts, David Williams, Clive Tadhunter, Sasha Tchekhovskoy, Francesco Ursini, Diana Worrall, and Nadia Zakamska. We acknowledge the useful comments by the referees that helped improving the manuscript. We also wish to thank Diego Altamirano, Piergiorgio Casella, Elia Chiaraluce, Sebastian Hoenig, Matt Middleton, Mayukh Pahari, Miguel Pérez-Torres and David Williams.

APPENDIX

A. ACRONYMS

tacama Large Millimeter/submillimeter Arra
thena Advanced Telescope for High ENergy Astrophysics
EHT Event Horizon Telescope
ELT Extremely Large Telescope
EVN European VLBI Network
eMERLIN extended Multi-Element Radio Linked Interferometer Network
eROSIT extended ROentgen Survey with an Imaging Telescope Array
FIRST Faint Images of the Radio Sky
ISM Interstellar medium
JWST James Webb Space Telescope
LINER Low-Ionization Nuclear Emission-line Region
LOF R LOw Frequency ARray
LSST Large Synoptic Survey Telescope
NVSS NRAO VLA Sky Survey
ngVL new-generation Very Large Array
QSO Quasi Stellar Object
SK Square Kilometre Array
SPIC Space Infrared Telescope for Cosmology and Astrophysics
VL Very Large Array
VLB Very Long Baseline Array
VLBI Very Long Baseline Interferometry
WFIRST Wide-Field InfraRed Survey Telescope

REFERENCES

Alexander, K. D., Berger, E., Guillochon, J., Zauderer, B. A., & Williams, P. K. G. 2016, ApJL, 819, L25

Alexander, K. D., Wieringa, M. H., Berger, E., Saxton, R. D., & Komossa, S. 2017, ApJ, 837, 153

Baldi, R. D., Behar, E., Laor, A., & Horesh, A. 2015, MNRAS, 454, 4277

Baldi, R. D., Williams, D. R. A., McHardy, I. M., et al. 2018, MNRAS, 476, 3478

Bally, J. 2016, ARA&A, 54, 491

Bally, J. 2007, Ap&SS, 311, 15

Barvainis, R., Lonsdale, C., & Antonucci, R. 1996, AJ, 111, 1431

Barvainis, R., Lehár, J., Birkinshaw, M., Falcke, H., & Blundell, K. M. 2005, ApJ, 618, 108

Batejat, F., Conway, J. E., Hurley, R., et al. 2011, ApJ, 740, 95

Baum, S. A., O'Dea, C. P., Dallacassa, D., de Bruyn, A. G., & Pedlar, A. 1993, ApJ, 419, 553
Behar, E., Baldi, R. D., Laor, A., et al. 2015, MNRAS, 451, 517
Behar, E., Vogel, S., Baldi, R. D., Smith, K. L., & Mushotzky, R. F. 2018, MNRAS, 478, 399
Begelman, M. C., Blandford, R. D., & Rees, M. J. 1984, Reviews of Modern Physics, 56, 255
Bell, M. E., Tzioumis, T., Uttley, P., et al. 2011, MNRAS, 411, 402
Belloni, T., Méndez, M., King, A. R., van der Klis, M., & van Paradijs, J. 1997, ApJL, 488, L109
Berger, E., Zauderer, A., Pooley, G. G., et al. 2012, ApJ, 748, 36
Blandford, R. D., & Königl, A. 1979, ApJ, 232, 34
Bloom, J. S., Giannios, D., Metzger, B. D., et al. 2011, Science, 333, 203
Blundell, K. M., & Beasley, A. J. 1998, MNRAS, 299, 165
Blundell, K. M., & Kuncic, Z. 2007, ApJL, 668, L103
Blundell, K. M., & Rawlings, S. 2001, ApJL, 562, L5
Blundell, K. M. 2003, NewAR, 47, 593
Blustin, A. J., & Fabian, A. C. 2009, MNRAS, 396, 1732
Bondi, M., Zamorani, G., Ciliegi, P., et al. 2018, A&A, 618, L8
Bontempi, P., Giroletti, M., Panessa, F., Orienti, M., & Doi, A. 2012, MNRAS, 426, 588
Bonzini, M., Mainieri, V., Padovani, P., et al. 2015, MNRAS, 453, 1079
Boroson T. A., Green R. F. 1992, ApJS, 80, 109
Brinkmann, W., Laurent-Muehleisen, S. A., Voges, W., et al. 2000, A&A, 356, 445
Capetti, A., Axon, D. J., Macchetto, F. D., Marconi, A., & Winge, C. 1999, ApJ, 516, 187
Capetti, A., Massaro, F., & Baldi, R. D. 2017, A&A, 598, A49
Carilli, C. 2015, Advancing Astrophysics with the Square Kilometre Array (AASKA14), 171
Chartas, G., Charlton, J., Eracleous, M., et al. 2009, NewAR, 53, 128
Chatterjee, R., Marscher, A. P., Jorstad, S. G., et al. 2009, ApJ, 704, 1689
Chi, S., Barthel, P. D., & Garrett, M. A. 2013, A&A, 550, A68
Chiaraluce, E., 2019, MNRAS, submitted
Christopoulou, P. E., Holloway, A. J., Ste en, W., et al. 1997, MNRAS, 284, 385
Condon, J. J. 1992, ARA&A, 30, 575
Condon, J. J., Kellermann, K. I., Kimball, A. E., Ivezić, Ž., & Perley, R. A. 2013, ApJ, 768, 37
Corbel, S., Nowak, M. A., Fender, R. P., Tzioumis, A. K., & Marko , S. 2003, A&A, 400, 1007
Corbel, S., Aussel, H., Broderick, J. W., et al. 2013, MNRAS, 431, L107
Cotton, W. D., Mason, B. S., Dicker, S. R., et al. 2009, ApJ, 701, 1872
Crenshaw D. M., Kraemer S. B., Boggess A., Maran S. P., Mushotzky R. F., & Wu C.-C. 1999, ApJ, 516, 750
Cseh, D., Miller-Jones, J. C. A., Jonker, P. G., et al. 2015, MNRAS, 452, 24
Dai, L., McKinney, J. C., Roth, N., Ramirez-Ruiz, E., & Miller, M. C. 2018, ApJL, 859, L20
Dewdney, P. E., Turner, W., Millenaar, R., et al. 2013, SKA1 System Baseline Design", Document number SKA-TEL-SKO-DD-001 Revision 1
Delvecchio, I., Smolčić, V., Zamorani, G., et al. 2017, A&A, 602, A3
Díaz Trigo, M., & Boirin, L. 2016, Astronomische Nachrichten, 337, 368
Díaz Trigo, M., Migliari, S., Miller-Jones, J. C. A., et al. 2017, A&A, 600, A8
Díaz Trigo, M., Altamirano, D., Dinçer, T., et al. 2018, A&A, 616, A23
Doi, A., Nakanishi, K., Nagai, H., Kohno, K., & Kameno, S. 2011, AJ, 142, 167
Doi, A., Kohno, K., Nakanishi, K., et al. 2013, ApJ, 765, 63
Falcke, H., & Biermann, P. L. 1995, A&A, 293, 665
Falcke, H., Nagar, N. M., Wilson, A. S., & Ulvestad, J. S. 2000, ApJ, 542, 197
Falcke, H., Körding, E., & Marko , S. 2004, A&A, 414, 895
Fanaro , B. L., & Riley, J. M. 1974, MNRAS, 167, 31P
Fender, R. P., Pooley, G. G., Durouchoux, P., Tilanus, R. P. J., & Brocksopp, C. 2000, MNRAS, 312, 853
Fender, R. P., Belloni, T. M., & Gallo, E. 2004, MNRAS, 355, 1105
Ferreira, J., Petrucci, P. O., Murphy, G., Zanni, C., & Henri, G. 2010, Accretion and Ejection in AGN: a Global View, 427, 49
Fukumura, K., & Kazanas, D., Contopoulos, I., & Behar, E. 2010, ApJ, 715, 636
Fukumura, K., Tombesi, F., Kazanas, D., et al. 2014, ApJ, 780, 120
Gallimore, J. F., Baum, S. A., & O'Dea, C. P. 2004, ApJ, 613, 794
Gallimore, J. F., Axon, D. J., O'Dea, C. P., Baum, S. A., & Pedlar, A. 2006, AJ, 132, 546
Genzel, R., Weitzel, L., Tacconi-Garman, L. E., et al. 1995, ApJ, 444, 129
Güdel, M., Audard, M., Smith, K. W., et al. 2002, ApJ, 577, 371

Guedel, M., & Benz, A. O. 1993, ApJL, 405, L63
Gürkan, G., Hardcastle, M., Best, P., et al. 2018, arXiv:1811.07933
Gurvits, L. I. 2018, arXiv:1810.01230
Giroletti, M., Panessa, F., Longinotti, A. L., et al. 2017, A&A, 600, A87
Giroletti, M., & Panessa, F. 2009, ApJL, 706, L260
Giroletti, M., Taylor, G. B., & Giovannini, G. 2005, ApJ, 622, 178
Gupta, A., Mathur, S., & Krongold, Y. 2015, ApJ, 798, 4
Haardt, F., & Maraschi, L. 1991, ApJL, 380, L51
Hagiwara, Y. 2007, AJ, 133, 1176
Hardcastle, M. J., & Looney, L. W. 2008, MNRAS, 388, 176
Harrison, C. M., Thomson, A. P., Alexander, D. M., et al. 2015, ApJ, 800, 45
Harrison, C. M., Costa, T., Tadhunter, C. N., et al. 2018, Nature Astronomy, 2, 198
Hartley, P., Jackson, N., Sluse, D., Stacey, H. R., & Vives Arias, H. 2019, arXiv:1901.05791
Heckman, T. M., Alexandro , R. M., Borthakur, S., Overzier, R., & Leitherer, C. 2015, ApJ, 809, 147
Heinz, S., & Sunyaev, R. A. 2003, MNRAS, 343, L59
Heywood, I., Blundell, K. M., & Rawlings, S. 2007, MNRAS, 381, 1093
Herrera Ruiz, N., Middelberg, E., Norris, R. P., & Maini, A. 2016, A&A, 589, L2
Herrero-Illana, R., Alberdi, A., Pérez-Torres, M. Á., et al. 2017, MNRAS, 470, L112
Ho, L. C., & Ulvestad, J. S. 2001, ApJS, 133, 77
Hwang, H.-C., Zakamska, N. L., Alexandro , R. M., et al. 2018, MNRAS, 477, 830
Inoue, Y., & Doi, A. 2014, PASJ, 66, L8
Inoue, Y., & Doi, A. 2018, ApJ, 869, 114
Doi, A., & Inoue, Y. 2016, PASJ, 68, 56
Jones, S., McHardy, I., Moss, D., et al. 2011, MNRAS, 412, 2641
Jones, S., McHardy, I., & Maccarone, T. J. 2017, MNRAS, 465, 1336
Kellermann, K. I., Sramek, R., Schmidt, M., Sha er, D. B., & Green, R. 1989, AJ, 98, 1195
Kellermann, K. I., Sramek, R. A., Schmidt, M., Green, R. F., & Sha er, D. B. 1994, AJ, 108, 1163
Kellermann, K. I., Condon, J. J., Kimball, A. E., Perley, R. A., & Ivezić, Ž. 2016, ApJ, 831, 168
Kharb, P., O'Dea, C. P., Baum, S. A., Colbert, E. J. M., & Xu, C. 2006, ApJ, 652, 177
Kharb, P., O'Dea, C. P., Baum, S. A., et al. 2014, MNRAS, 440, 2976
Kharb, P. 2018, Revisiting narrow-line Seyfert 1 galaxies and their place in the Universe. 9-13 April 2018. Padova Botanical Garden, Italy, id.23, 23
King, A. L., Miller, J. M., Cackett, E. M., et al. 2011, ApJ, 729, 19
King, A. L., Miller, J. M., Reynolds, M. T., et al. 2013, ApJL, 774, L25
King, A. L., Lohfink, A., & Kara, E. 2017, ApJ, 835, 226
Körding, E., Falcke, H., & Corbel, S. 2006, A&A, 456, 439
Körding, E., Rupen, M., Knigge, C., et al. 2008, Science, 320, 1318
Kukula, M. J., Holloway, A. J., Pedlar, A., et al. 1996, MNRAS, 280, 1283
Kukula, M. J., Dunlop, J. S., Hughes, D. H., & Rawlings, S. 1998, MNRAS, 297, 366
Laing, R. A., & Bridle, A. H. 2013, MNRAS, 432, 1114
Laor A., Brandt W. N. 2002, ApJ, 569, 641
Laor, A., & Behar, E. 2008, MNRAS, 390, 847
Laor, A., Baldi, R. D., & Behar, E. 2019, MNRAS, 482, 5513
Leipski, C., Falcke, H., Bennert, N., & Hüttemeister, S. 2006, A&A, 455, 161
Lena, D., Robinson, A., Storchi-Bergman, T., et al. 2015, ApJ, 806, 84
Longinotti, A. L., Krongold, Y., Guainazzi, M., et al. 2015, ApJL, 813, L39
Liu, T., Wang, J.-X., Yang, H., Zhu, F.-F., & Zhou, Y.-Y. 2014, ApJ, 783, 106
Maini, A., Prandoni, I., Norris, R. P., Giovannini, G., & Spitler, L. R. 2016, A&A, 589, L3
Maiolino, R., Krabbe, A., Thatte, N., & Genzel, R. 1998, ApJ, 493, 650
Malzac, J., Belloni, T., Spruit, H. C., & Kanbach, G. 2003, A&A, 407, 335
Malzac, J., Merloni, A., & Fabian, A. C. 2004, MNRAS, 351, 253
Marko , S., Falcke, H., & Fender, R. 2001, A&A, 372, L25
Marscher, A. P., Jorstad, S. G., Gómez, J.-L., et al. 2002, Nature, 417, 625
Mattila, S., Pérez-Torres, M., Efstathiou, A., et al. 2018, Science, 361, 482
Merloni, A., & Fabian, A. C. 2002, MNRAS, 332, 165
Merloni, A., Heinz, S., & di Matteo, T. 2003, MNRAS, 345, 1057
Middelberg, E., Roy, A. L., Nagar, N. M., et al. 2004, A&A, 417, 925
Mirabel, I. F., Dhawan, V., Chaty, S., et al. 1998, A&A, 330, L9
Morganti, R., Oosterloo, T., Oonk, J. B. R., Frieswijk, W., & Tadhunter, C. 2015, A&A, 580, A1

Mullaney, J. R., Alexander, D. M., Fine, S., et al. 2013, MNRAS, 433, 622
Mundell, C. G., Wrobel, J. M., Pedlar, A., & Gallimore, J. F. 2003, ApJ, 583, 192
Mundell, C. G., Ferruit, P., Nagar, N., & Wilson, A. S. 2009, ApJ, 703, 802
Murphy, E., Sargent, M., Beswick, R., et al. 2015, Advancing Astrophysics with the Square Kilometre Array (AASKA14), 85
Murphy, E. J., Carilli, C. L., & ngVLA Science Working Groups 2017, American Astronomical Society Meeting Abstracts #229, 229, 348.08
Muxlow, T. W. B., Pedlar, A., Wilkinson, P. N., et al. 1994, MNRAS, 266, 455
Nagar, N. M., Wilson, A. S., & Falcke, H. 2001, ApJL, 559, L87
Nagar, N. M., Falcke, H., Wilson, A. S., & Ulvestad, J. S. 2002, A&A, 392, 53
Nagar, N. M., Falcke, H., Wilson, A. S., & Ho, L. C. 2002, NewAR, 46, 225
Nardini, E., Reeves, J. N., Go ord, J., et al. 2015, Science, 347, 860
Nyland, K., Young, L. M., Wrobel, J. M., et al. 2016, MNRAS, 458, 2221
Nims, J., Quataert, E., & Faucher-Giguère, C.-A. 2015, MNRAS, 447, 3612
Neupert, W. M. 1968, ApJL, 153, L59
Olsson, E., Aalto, S., Thomasson, M., & Beswick, R. 2010, A&A, 513, A11
Orienti, M., D'Ammando, F., Giroletti, M., Giovannini, G., & Panessa, F. 2015, Advancing Astrophysics with the Square Kilometre Array (AASKA14), 87
Osorio, M., Díaz-Rodríguez, A. K., Anglada, G., et al. 2017, ApJ, 840, 36
Padovani, P., Miller, N., Kellermann, K. I., et al. 2011, ApJ, 740, 20
Padovani, P., Bonzini, M., Kellermann, K. I., et al. 2015, MNRAS, 452, 1263
Padovani, P. 2016, A&A Rv, 24, 13
Padovani P., et al., 2017, A&ARv, 25, 2
Padovani, P. 2017, Nature Astronomy, 1, 0194
Panessa, F., Barcons, X., Bassani, L., et al. 2007, A&A, 467, 519
Panessa, F., & Giroletti, M. 2013, MNRAS, 432, 1138
Panessa, F., Tarchi, A., Castangia, P., et al. 2015, MNRAS, 447, 1289
Paragi, Z., Godfrey, L., Reynolds, C., et al. 2015, Advancing Astrophysics with the Square Kilometre Array (AASKA14), 143
Pasham, D. R., & van Velzen, S. 2018, ApJ, 856, 1
Pedlar, A., Kukula, M. J., Longley, D. P. T., et al. 1993, MNRAS, 263, 471
Pérez-Torres, M. A., Romero-Cañizales, C., Alberdi, A., & Polatidis, A. 2009, A&A, 507, L17
Pietka, M., Fender, R. P., & Keane, E. F. 2015, MNRAS, 446, 3687
Plotkin, R. M., Marko , S., Kelly, B. C., Körding, E., & Anderson, S. F. 2012, MNRAS, 419, 267
Ponti, G., Fender, R. P., Begelman, M. C., et al. 2012, MNRAS, 422, L11
Pounds, K. A. 2014, MNRAS, 437, 3221
Price, D. J., Pringle, J. E., & King, A. R. 2003, MNRAS, 339, 1223
Raginski, I., & Laor, A. 2016, MNRAS, 459, 2082
Reynolds, S. P. 1982, ApJ, 256, 13
Roberts, T. P. 2007, Ap&SS, 311, 203
Rosario, D. J., Burtscher, L., Davies, R., et al. 2013, ApJ, 778, 94
Roy, A. L., Wilson, A. S., Ulvestad, J. S., & Colbert, J. M. 2000, EVN Symposium 2000, Proceedings of the 5th european VLBI Network Symposium, 7
Russell, D. M., Miller-Jones, J. C. A., Maccarone, T. J., et al. 2011, ApJL, 739, L19
Salvato, M., Greiner, J., & Kuhlbrodt, B. 2004, ApJL, 600, L31
Sargent, M. T., Schinnerer, E., Murphy, E., et al. 2010, ApJS, 186, 341
Shapiro, S. L., Lightman, A. P., & Eardley, D. M. 1976, ApJ, 204, 187
Singh, V., Ishwara-Chandra, C. H., Wadadekar, Y., Beelen, A., & Kharb, P. 2015, MNRAS, 446, 599
Steenbrugge, K. C., Heywood, I., & Blundell, K. M. 2010, MNRAS, 401, 67
Steenbrugge, K. C., Jolley, E. J. D., Kuncic, Z., & Blundell, K. M. 2011, MNRAS, 413, 1735
Sopp, H. M., & Alexander, P. 1991, MNRAS, 251, 14P
Tchekhovskoy, A., Narayan, R., & McKinney, J. C. 2011, MNRAS, 418, L79
Terashima, Y., & Wilson, A. S. 2003, ApJ, 583, 145
Tetarenko, A. J., Sivako , G. R., Miller-Jones, J. C. A., et al. 2018, MNRAS, in publication
Tetarenko, A. J., Bremer, M., Bright, J., et al. 2018, The Astronomer's Telegram, 11440,
Thean, A., Pedlar, A., Kukula, M. J., Baum, S. A., & O'Dea, C. P. 2001, MNRAS, 325, 737
Tobin, J. J., Dunham, M. M., Looney, L. W., et al. 2015, ApJ, 798, 61
Tombesi, F., Cappi, M., Reeves, J. N., et al. 2010, A&A, 521, A57

Tombesi, F., Sambruna, R. M., Reeves, J. N., Reynolds, C. S., & Braito, V. 2011, MNRAS, 418, L89

Ulvestad, J. S., & Ho, L. C. 2001, ApJ, 558, 561

Ulvestad, J. S., Antonucci, R. R. J., & Barvainis, R. 2005, ApJ, 621, 123

van den Eijnden, J., Degenaar, N., Russell, T. D., et al. 2018, MNRAS, 473, L141

van Haarlem, M. P., Wise, M. W., Gunst, A. W., et al. 2013, A&A, 556, A2

van Velzen, S., Anderson, G. E., Stone, N. C., et al. 2016, Science, 351, 62

Veilleux, S., Cecil, G., Bland-Hawthorn, J., et al. 1994, ApJ, 433, 48

Veilleux, S., Cecil, G., & Bland-Hawthorn, J. 2005, ARA&A, 43, 769

Wang, R., Wu, X.-B., & Kong, M.-Z. 2006, ApJ, 645, 890

White, S. V., Jarvis, M. J., Kalfountzou, E., et al. 2017, MNRAS, 468, 217

Williams, D. R. A., McHardy, I. M., Baldi, R. D., et al. 2017, MNRAS, 472, 3842

Wrobel, J. M. 2000, ApJ, 531, 716

Yuan, F., Marko , S., & Falcke, H. 2002, A&A, 383, 854

Yuan, F., Quataert, E., & Narayan, R. 2003, ApJ, 598, 301

Yuan, F., & Narayan, R. 2014, ARA&A, 52, 529

Yuan, Q., Wang, Q. D., Lei, W.-H., Gao, H., & Zhang, B. 2016, MNRAS, 461, 3375

Zakamska, N. L., & Greene, J. E. 2014, MNRAS, 442, 784

Zakamska, N. L., Lampayan, K., Petric, A., et al. 2016a, MNRAS, 455, 4191

Zakamska, N. L., Hamann, F., Pâris, I., et al. 2016b, MNRAS, 459, 3144